JOURNAL OF MATERIALS SCIENCE 35 (2000) 399–409

Study on the α_2/γ interfacial structures in a two-phase ($\alpha_2+\gamma$) alloy deformed at elevated temperature

JINGUO WANG*
Lawrence Livermore National Laboratory, Chemistry and Materials Science, P.O. Box 808, L-370, Livermore, CA 94551-9900, USA
E-mail: wang21@llnl.gov

LICHUN ZHANG, GUOLIANG CHEN
State Key Laboratory for Advanced Metals and Materials, University of Science and Technology Beijing, Beijing, 100083, People's Republic of China

HENQIANG YE
Laboratory of Atomic Imaging of Solids, Institute of Metal Research, Academia Sinica, Shenyang, 110015, People's Republic of China

The details of structure modification on α_2/γ interface induced by deformation in a hot-deformed Ti-45Al-10Nb alloy were investigated by conventional and high-resolution transmission electron microscopy. A new type of dislocation ledge containing 1/3[111] partials was identified. The Burgers vectors of these dislocation ledges were determined to be 1/2[110] or 1/2⟨101]. The formation mechanism of this new type of dislocation ledge is discussed. Also, two types of hot deformation induced α_2/γ interfaces, coherent interfaces with high density of ledges and misoriented semi-coherent α_2/γ interfacial boundaries were observed. For the misoriented semi-coherent α_2/γ interfaces, the density of dislocation ledges in these interfaces increases with the misoriented angle between the $(111)_\gamma$ and $(0001)_{\alpha 2}$ planes, and 1/3[111] partial dislocations were involved in all the dislocation ledges. The formation mechanism of these deformation-induced α_2/γ interfaces were discussed related to the role of α_2/γ interfaces adjusting the deformation as a dislocation sink absorbing the slipping dislocations in the γ phase. Moreover, misoriented semi-coherent α_2/γ interface related deformation twinning and structure transformation induced by deformation were analyzed and discussed related to the role of α_2/γ interfaces as a dislocation source during deformation.

1. Introduction

Considerable attention has been focused on two-phase (TiAl + Ti_3Al) intermetallic alloys for application in the aerospace industry because the two-phase microstructure in Ti-rich alloys consisting of primary TiAl(γ) phase and lamellar $Ti_3Al(\alpha_2)$ + TiAl structure can significantly improve the room-temperature ductility [1–3]. Several mechanisms have been put forward to account for this improvement in ductility [4]. Factors such as the gettering of interstitial impurities by α_2-phase, the increased mobility of 1/2⟨110] and 1/6⟨112] dislocations in TiAl in the presence of Ti_3Al phase, the fineness of the microstructure, and the uniform deformation of the lamellar structure are believed to contribute to enhanced ductility. It is now well known that the two-phase lamellar structure can be significantly modified by thermomechanical and heat treatments; so the relationships between microstructure and mechanical properties are now being evaluated by many research groups in order to obtain further improvement [4–7].

In the two-phase TiAl alloys, the orientation relationships between neighboring α_2-Ti_3Al and γ-TiAl lamellae are well defined as $(0001)_{\alpha 2}//\{111\}_\gamma$ and $\langle 11\bar{2}0\rangle_{\alpha 2}//\langle 110\rangle_\gamma$ with the interface plane $(0001)_{\alpha 2}//\langle 111\rangle_\gamma$ [8]. Some attention was paid to the study of these interfaces. For example, Kawabata, Tdano and Izumi [9] observed slip along Ti_3Al/TiAl interfaces, Hall and Huang [1] found a high density of dislocations in the interfaces, and Huang and Hall [10] also pointed out that numerous interfaces enhance or allow deformation of the transformed Ti_3Al + TiAl lamellae.

More intensive studies on the lamellar interfaces through transmission electron microscopy (TEM) have

* Author to whom all correspondence should be addressed; *Present address*: Department of Chemical and Biochemical Engineering and Materials Science, 916 Engineering Tower, University of California Irvine, Irvine, CA 92697-2575.

been carried out [11–16]. While some differences existed in the results given by these authors, a common conclusion obtained was that the TiAl/Ti_3Al interfaces contained closely spaced (<50 nm) interfacial dislocations. The Burgers vectors, line direction and spacing of these dislocations were determined to be controlled by the misfit of the interfaces. It is suggested that the glide of the interfacial dislocations at lower temperatures as well as the migration of the interfaces at high temperatures play a significant role in improving the ductility of the two-phase alloy [16]. The α_2/γ interfaces in two-phase ($\gamma + \alpha_2$) titanium aluminides were also investigated by many workers through high resolution transmission electron microscopy (HREM) [17–30], the main finding is the ledge structure existing at the interfaces. Most of the authors found Burgers vectors $1/6\langle 11\bar{2}\rangle$ dislocations associated with two atomic plane ledges. Meanwhile, four atomic plane ledges are also observed in TiAl/Ti_3Al alloy [24]. Two types of partial dislocation ledges, 90° and 30° $1/6\langle 11\bar{2}\rangle$ partial dislocation ledges, have been reported [29]. It is realized that α_2/γ interfaces were structurally coherent between dislocation ledges and chemically discontinuous across the interface.

Ti-45Al-10Nb is a high performance alloy with excellent high temperature strength and oxidation resistance [31]. As a part of our systematic continual researches on the deformation induced microstructures and phase transitions in Ti-Al-Nb ternary intermetallic alloys [31–40]. This paper reports high-resolution transmission electron microscopy (HREM) observations of the deformation-induced α_2/γ interfacial structures in a hot-deformed Ti-45Al-10Nb alloy.

2. Experimental procedure

Alloy Ti-45Al-10Nb (in at %) ingot was prepared by non-consumable electrode arc-melting in a purified argon atmosphere. The as-cast ingot was wrapped in steel foil and annealed at 1250 °C for 30 min, followed by quasi-isothermal forging to more than 40% reduction. The temperature of the forge hammer was 1050 °C and the forging speed was about 5×10^{-1} s^{-1}. The forged ingot was cooled to room temperature in air.

Conventional transmission electron microscope (TEM) observations and high resolution transmission electron microscope (HREM) investigations were performed on the forged material. TEM foils were prepared by either twin jet polishing or ion-milling. Diffraction studies and microstructure observations were conducted using JEOL-200CX or Philip 420. HREM was performed in a JEOL-2000EXII electron microscope operating at 200 kV with a spherical aberration coefficient of 0.7 mm. Interfaces in the samples were examined in either $\langle 1\bar{1}0]$ or $\langle 10\bar{1}]$ orientations with the α_2/γ interfaces edge on.

3. Results

3.1. Microstructure of the forged alloy

Fig. 1 shows the X-ray diffraction (XRD) results of the quasi-isothermal forged Ti-45Al-10Nb alloy. It can be clearly seen that the phases available in the alloy are γ-TiAl and α_2-Ti_3Al, no β or B2 phases are found. Due to the fact that Nb atoms added to TiAl or Ti_3Al as substitution atoms occupying preferentially on the Ti sublattice [41], we can analyze the phase constitution and microstructure of the Ti-45Al-10Nb alloy approximately using the binary Ti-Al phase diagram. The quasi-isothermal forging temperature is in the range of 1050–1200 °C, it is close to the eutectoid temperature. Such hot-working generally results in a nearly lamellar microstructure. The lamellar structure is deformed and is simultaneously dynamically recovered or partially recrystallized. Dynamic recrystallization of deformed lamellar structure has been found to occur preserving its lamellar morphology (see Fig. 2). The effects of hot-deformation on the structure of the α_2/γ interface

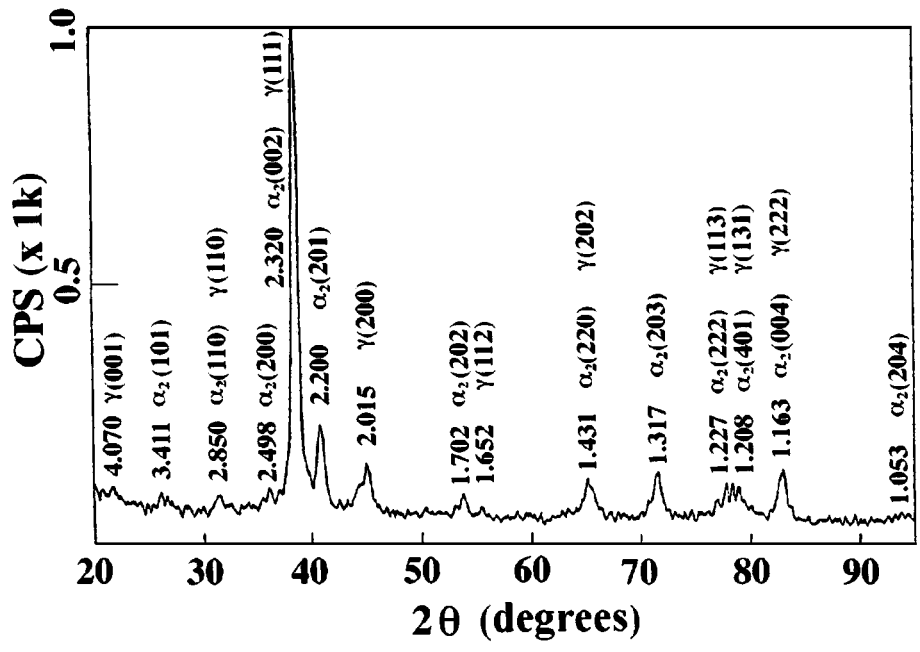

Figure 1 X-ray diffraction pattern of the hot-deformed Ti-45Al-10Nb alloy.

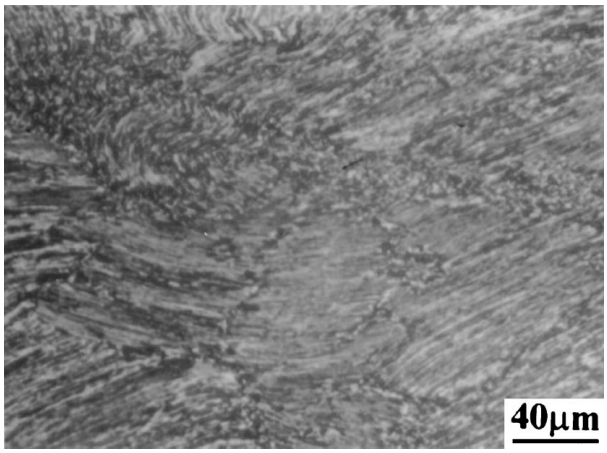

Figure 2 Optical microstructure of the hot-deformed Ti-45Al-10Nb alloy.

and the characteristics of the interfacial partial dislocations are analyzed by using HREM as described in the followings.

3.2. Characteristics of ledge dislocations at the α_2/γ interface

Figs 3a and b show two γ_B/α_2 interfaces which are indicated as interfaces I and II respectively, because the orientation relationships of $(0001)_{\alpha 2}//\{111\}_\gamma$ and $\langle 11\bar{2}0\rangle_{\alpha 2}//\langle 110\rangle_\gamma$ could give rise to six possible orientation variants of $\langle 110\rangle_\gamma$ with respect to $\langle 11\bar{2}0\rangle_{\alpha 2}$ [11], here the symbols γ_A, γ_B, γ_C, γ_D, γ_E and γ_F are used to distinguish the six γ variants with [110], [1$\bar{1}$0], [101], [10$\bar{1}$], [011], [01$\bar{1}$] orientation respectively [42–45]. Ledges with two atomic plane $(111)\gamma$ or $(0001)_{\alpha 2}$ high were observed in both interfaces and two such ledges are indicated by A and B in the interfaces I and II respectively. Following the analysis procedures for drawing the Burgers circuits described by Howe *et al*. [46], two different types of Burgers circuit that can be used to distinguish between 90° and 30° $1/6\langle 11\bar{2}\rangle$ partial dislocation ledges are illustrated in Figs 3c and d for ledges A and B respectively. The characteristics of ledge dislocations in ledges A and B can be determined to be 90° and 30° $1/6\langle 11\bar{2}\rangle$ dislocation ledges. The Burgers vector of the 90° $1/6\langle 11\bar{2}\rangle$ partial dislocation lies perpendicular to the [110] electron beam direction with $1/6[11\bar{2}]$, whereas for the 30° $1/6\langle 11\bar{2}\rangle$ partial dislocation the Burgers vector lies at an angle of 30° to the electron beam and is either $1/6[\bar{2}11]$ or $1/6[\bar{1}21]$. The sharpness of the bright dots which lie on the atomic columns seems to indicate that the 30° partial dislocation core is localized, whereas the core of 90° partial dislocation appears highly delocalized or diffuse. The diffuseness of the 90° partial dislocation core may be

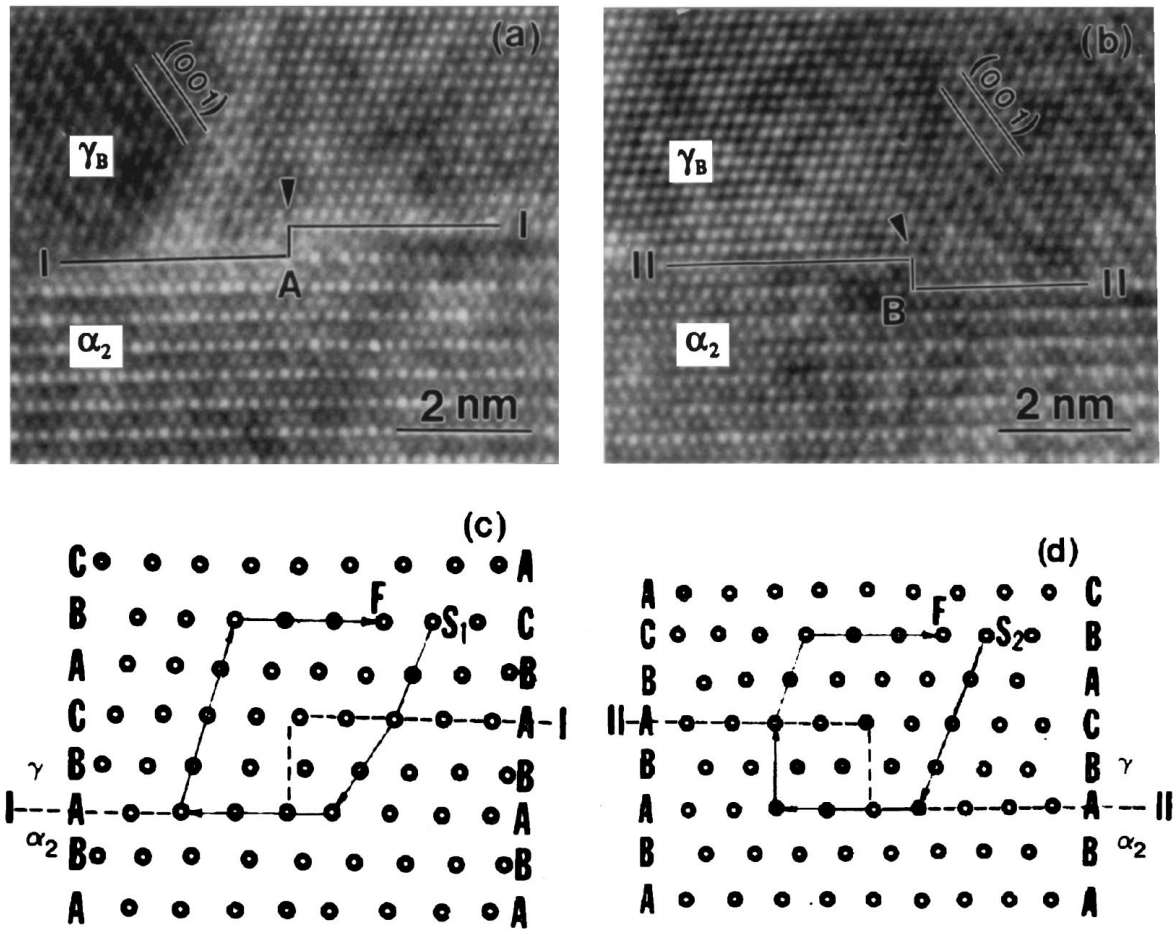

Figure 3 HREM images of ledges at γ/α_2 interfaces with $1/6\langle 11\bar{2}\rangle$ partial dislocations (a) 90° (edge) $1/6\langle 11\bar{2}\rangle$ partial, (b) 30° (screw) $1/6\langle 11\bar{2}\rangle$ partial, (c) and (d) schematic atomic arrangement at the ledges of A and B shown in (a) and (b) respectively. In (c) and (d) two Burgers circuit are also shown that can be used to distinguish 90° and 30° $1/6\langle 11\bar{2}\rangle$ partial dislocations respectively. S_1 and S_2 indicate the start of the 90° (edge) and 30° (screw) Burgers circuits, respectively, while F indicate the finish of the circuits.

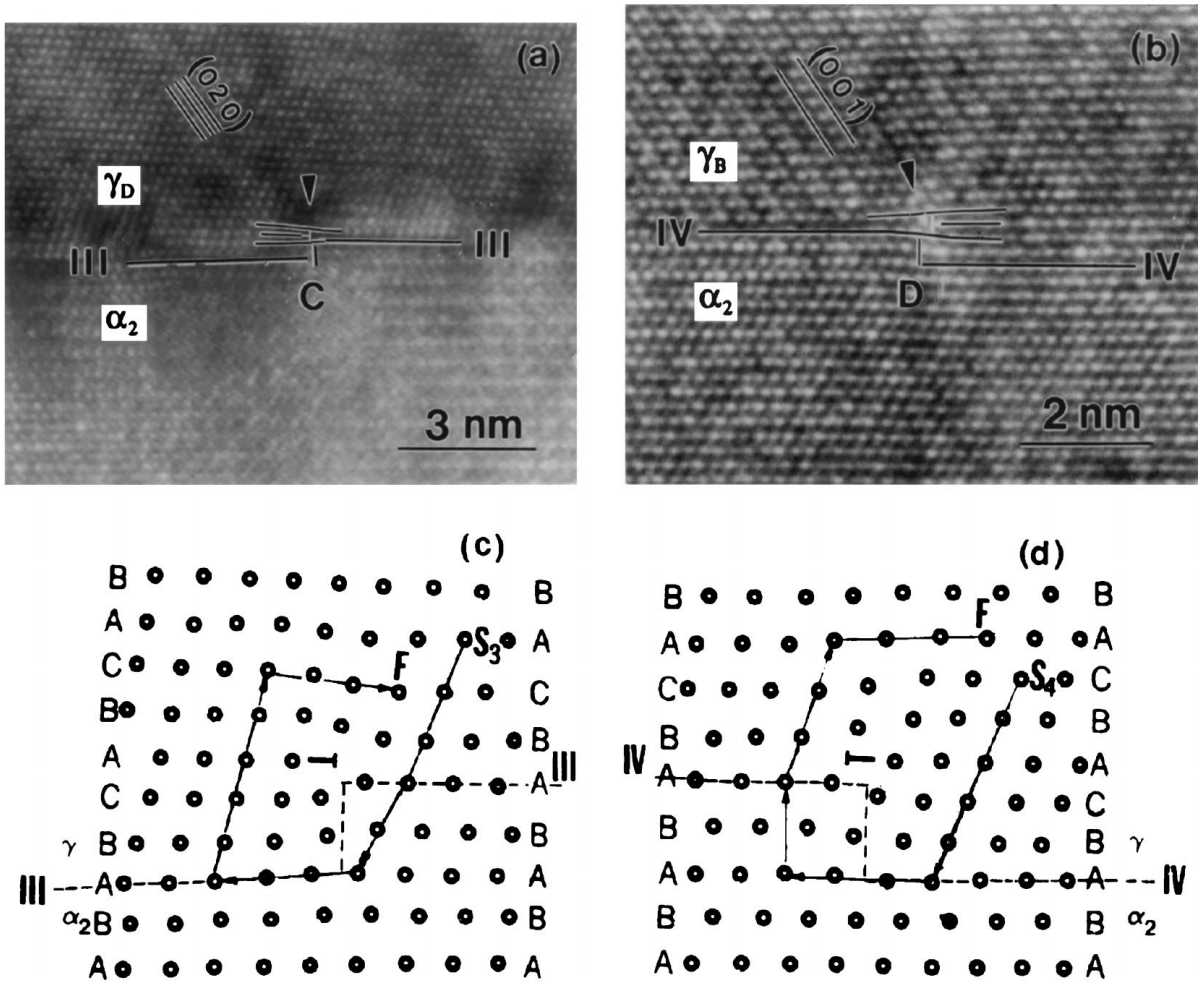

Figure 4 HREM images of ledges at γ/α_2 interfaces with $1/3[111] + 1/6\langle 11\bar{2}\rangle$ partial dislocations (a) 90° (edge) $1/6\langle 11\bar{2}\rangle$ partial $+1/3[111]$ partial, (b) 30° (screw) $1/6\langle 11\bar{2}\rangle$ partial $+1/3[111]$ partial, (c) and (d) schematic atomic arrangement at the ledges of C and D shown in (a) and (b) respectively. In (c) and (d) two Burgers circuits are also shown that can be used to distinguish 90° and 30° $1/6\langle 11\bar{2}\rangle$ partial dislocations respectively. S_3 and S_4 indicate the start of the 90° (edge) and 30° (screw) Burgers circuits, respectively, while F indicates the finish of the circuits.

due to the presence of a high density of kinks along the ledge as a result of growth-induced deviation of the ledge away from the exact {110} orientation [29].

Fig. 4 also shows γ_D/α_2 and γ_B/α_2 interfaces which are indicated as interfaces III and IV, respectively. Ledges that were three atomic plane $(111)_\gamma$ or $(0001)_{\alpha 2}$ high were observed in both interfaces and two such ledges are indicated by C and D in the interfaces III and IV respectively. Figs 4c and d illustrate the two different types of Burgers circuit for ledges C and D using the drawing methods of 90° and 30° $1/6\langle 11\bar{2}\rangle$ partial dislocation ledges respectively. Both Burgers circuits lead to a closure failure. However, it is important to note that the finishing points of these two circuits do not locate at the same (111) plane as the start of the circuits, which is different from the situation in Figs 3c and d. Considering that not all the projected atom positions in these $\langle 110\rangle//\langle 11\bar{2}0\rangle$ models are coplanar, i.e. every other atom actually lies in a plane which is slightly above or below the plane of the figure, as can be seen by examining a $\langle 110\rangle$ $L1_0$ lattice, the Burgers vectors of dislocation ledges C and D can be determined to be $1/2\langle 101]$. Furthermore, it can be seen clearly from the HREM images that evident differences exist between ledges C, D and ledges A, B. An extra half atomic plane exists in the ledges C and D. This means the there is a $1/3[111]$ partial dislocation at the ledge. So the characteristics of ledge dislocations in ledges C and D can be both considered as: $1/6[1\bar{2}1] + 1/3[111] = 1/2[101]$. For ledge C, the partial dislocation $1/6[1\bar{2}1]$ lies perpendicular to the beam direction $[\bar{1}01]$, it is a 90° dislocation. For ledge D, the partial dislocation $1/6[1\bar{2}1]$ lies at an angle of 30° to the beam direction $[\bar{1}10]$, it is a 30° dislocation. Thus the characteristics of whole ledge dislocations in ledges C and D are 90° $1/6\langle 11\bar{2}\rangle$ dislocation + $1/3[111]$ partial dislocation and 30° $1/6\langle 11\bar{2}\rangle$ dislocation + $1/3[111]$ partial dislocation respectively. Figs 4c and d illustrate the stacking sequences of the α_2-Ti_3Al and γ-TiAl at the interface resulting from the ledge dislocations C and D respectively.

It can also be seen from Fig. 4 that the $1/6\langle 11\bar{2}\rangle$ partial dislocation and the $1/3[111]$ partial dislocation do not lie at the same (111) plane, the $1/6\langle 11\bar{2}\rangle$ partial alters the interfacial plane from A to C stacking sequence, the $1/3[111]$ partial lies one plane above this plane. The $1/3[111]$ partial is always in the γ phase.

3.3. Deformation-induced changes in coherent α_2/γ interfaces

As mentioned above, since the $\langle \bar{1}10]_\gamma$ and $\langle 0\bar{1}1]_\gamma$ directions in the γ phase with $L1_0$ tetragonal structure

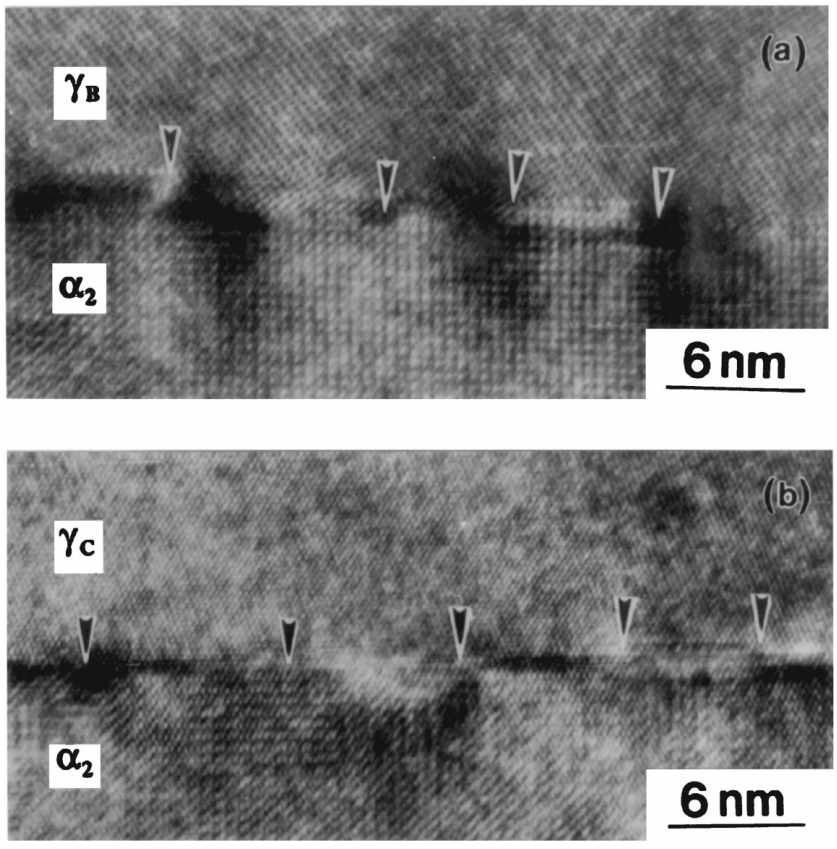

Figure 5 HREM images of the typical coherent α_2/γ interfaces under the quasi-isothermal forged state. (a) and (b) are γ_B/α_2 and γ_C/α_2 interfaces respectively.

are not equivalent, α_2/γ interfaces may have two categories from the morphology, i.e. γ_A/α_2, γ_B/α_2 ($\langle 1\bar{1}0]_\gamma // \langle 11\bar{2}0\rangle_{\alpha 2}$) and γ_C/α_2, γ_D/α_2 ($\langle 101]_\gamma // \langle 11\bar{2}0\rangle_{\alpha 2}$). Typical structure of the coherent α_2/γ interfaces under the quasi-isothermal forged state observed by HREM is shown in Fig. 5, where (a) and (b) are γ_B/α_2 and γ_C/α_2 interfaces respectively. These interfaces are atomically flat and coherent between ledges. The ledges are always two atomic planes $(111)_\gamma$ high. Very dark contrast in the head of the ledges reveals that high stress exists at the ledges in the interface. The mean distance between ledges is less than 10 nm. Compared with the α_2/γ interfaces observed in the annealed alloys [18, 19, 21], we can find that:

(1) the hot deformation-induced ledges in the α_2/γ interfaces have similar height (two atomic planes) with the growth ledges in the annealed alloys.

(2) deformation stress at the hot deformation-induced ledges is higher than the misfit stress in the annealed alloys, it is difficult for the ledges to be clearly imaged in HREM for the hot-worked alloys.

(3) the density of the hot deformation-induced ledges on α_2/γ interfaces is higher than that of the transformation growth ledges in annealed alloys (the mean distances between the transformation growth ledges in the α_2/γ interfaces of annealed alloys were 15–30 nm according to different works [18, 19, 21]). This suggests that more mismatch can be accommodated by the deformation dislocations in the hot-worked state than by growth misfit dislocations in the annealed state.

(4) 1/3[111] partial dislocations can be observed at some ledges in α_2/γ interfaces (see Fig. 4).

3.4. Deformation induced misoriented semi-coherent α_2/γ interfaces

Owing to the tetragonality of $L1_0$-TiAl phase ($c/a \approx 1.02$), the $\langle 110]$ direction in the TiAl phase has been found to be exactly parallel to the $\langle 11\bar{2}0\rangle$ direction in the Ti_3Al phase, but there is a rotation of 0.2–0.3° between the corresponding $\langle 101]$ in TiAl and $\langle 11\bar{2}0\rangle$ in Ti_3Al about the [111] direction in the TiAl phase. The mismatches stemming from the tetragonality of the TiAl phase and from the difference between the lattice constants of the TiAl and Ti_3Al phases result in the transformation misfit ledges in the coherent α_2/γ interfaces of annealing alloys [21, 30]. In the hot-deformed Ti-45Al-10Nb alloy, besides the interfaces with higher density of ledges which are observed in the last part, there also exists an unique type of misoriented semi-coherent α_2/γ interface. In these interfaces, the orientation relationship $\langle 10\bar{1}]_\gamma // \langle 11\bar{2}0\rangle_{\alpha 2}$ remains unchanged, but a misoriented angle between $(111)\gamma$ and $(0001)_{\alpha 2}$ planes exists. Fig. 6 shows such α_2/γ interfaces with three different angles; all these interfaces were imaged along the $\langle 10\bar{1}]_\gamma // \langle 11\bar{2}0\rangle_{\alpha 2}$ directions. Figs 7a–c are the local enlargements of interfaces in Figs 6a–c respectively. In Figs 6a and 7a, it is a γ_C/α_2 interface, the orientation relationship between the γ and the α_2 phase is $[10\bar{1}]_\gamma // [11\bar{2}0]_{\alpha 2}$ and $(111)_\gamma \wedge (0001)_{\alpha 2} \approx 2.5°$. Ledges that were two or three $(111)_\gamma$ or $(0001)_{\alpha 2}$ high were observed and some

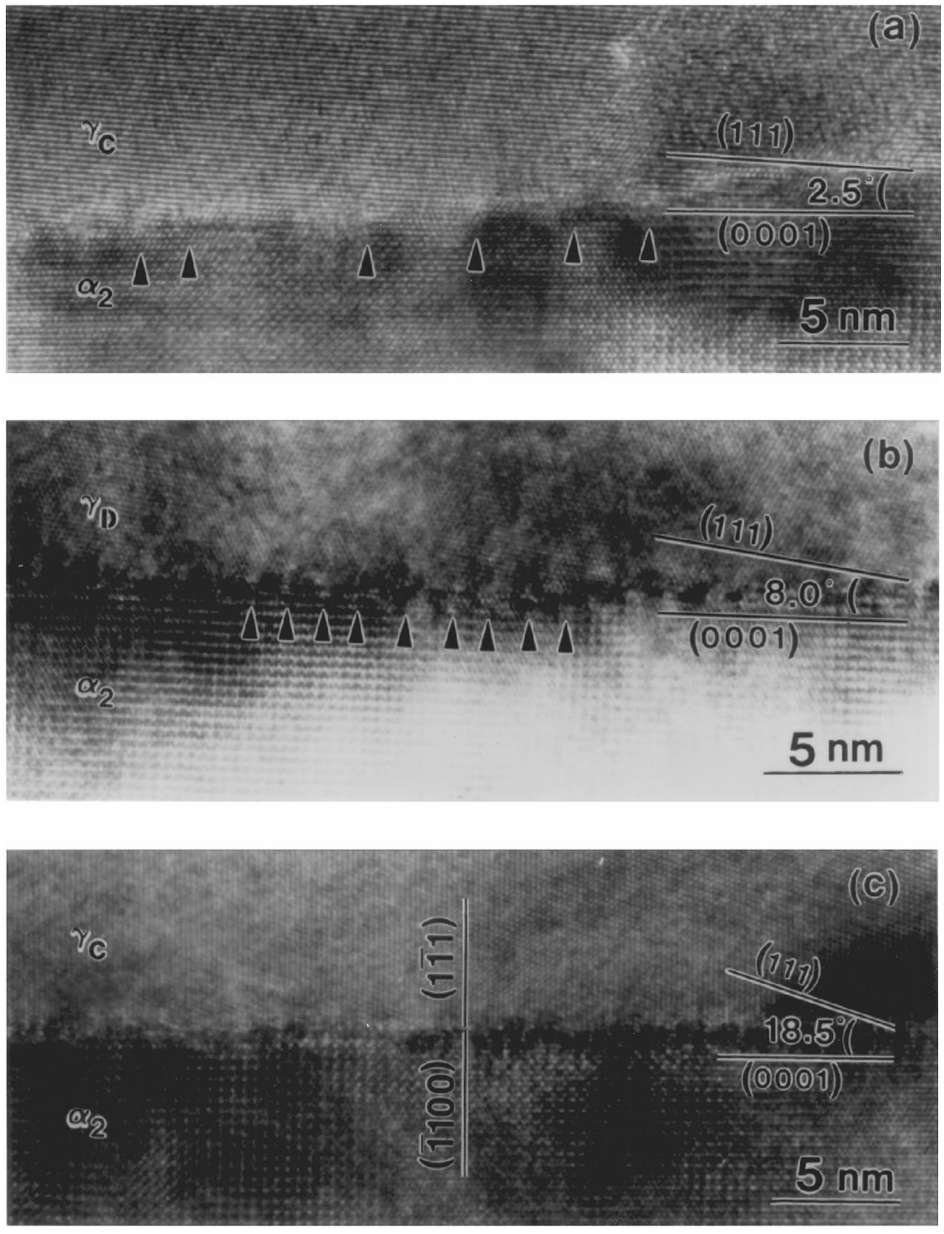

Figure 6 HREM images of the misoriented semi-coherent α_2/γ interfaces with different misoriented angle between $(111)_\gamma$ and $(0001)_{\alpha 2}$ planes. (a) 2.5°, (b) 8.0° and (c) 18.5°.

ledges are indicated by arrows. 1/3[111] partial dislocations can be observed at the dislocation ledges in Fig. 7a. The mean distance of these ledges is about 4.6 nm. Very dark contrast near the ledges reveals that high stress exist at the dislocation ledges. Figs 6b and 7b show a γ_D/α_2 interface, the orientation relationship between γ and α_2 phase is $[\bar{1}01]_\gamma // [11\bar{2}0]_{\alpha 2}$ and $(111)_\gamma \wedge (0001)_{\alpha 2} \approx 8°$. Ledges that were two or three $(111)_\gamma$ or $(0001)_{\alpha 2}$ high were observed and some ledges are indicated by arrows. Also, 1/3[111] partial dislocations can be observed at the ledges (Fig. 7b). The mean distance of the ledges is about 1.8 nm. The density of ledges in this interface is higher than that in Fig. 6a and the stress existing at the ledges in this interface is also higher than that in Fig. 6a. Figs 6c and 7c show another γ_C/α_2 interface, the orientation relationship between γ and α_2 phase is $[\bar{1}01]_\gamma // [11\bar{2}0]_{\alpha 2}$ and $(111)_\gamma \wedge (0001)_{\alpha 2} \approx 18.5°$, in fact, such an orientation relationship is crystallographically similar to $[10\bar{1}]_\gamma // [11\bar{2}0]_{\alpha 2}$ and $(111)_\gamma // (1100)_{\alpha 2}$. The interface plane seems flat and parallel to the $(0001)_{\alpha 2}$ plane (but makes an angle of 18.5° with the $(111)_\gamma$ plane) in a macroscale. Since the difference between the $d_{(1100)\alpha 2}$ (=0.288 nm) of the α_2 phase and the $d_{(111)\gamma}$ (=0.231 nm) of the γ phase is very large, it reaches 20%, and a high density of interfacial dislocations will be formed in the interface, the formation of these interfacial dislocations can be considered as introducing an extra half atomic plane $(111)_\gamma$ on every four to five $(111)_\gamma$ planes. The characteristic of these interfacial dislocations is the 1/3[111] partial dislocation. Due to the very high stress resulting from high mismatches, it is very difficult to image the interface clearly in HREM.

In summary, in the quasi-isothermal forged Ti-45Al-10Nb alloy, besides the existence of normal coherent α_2/γ interfaces with ledges of two atomic planes which

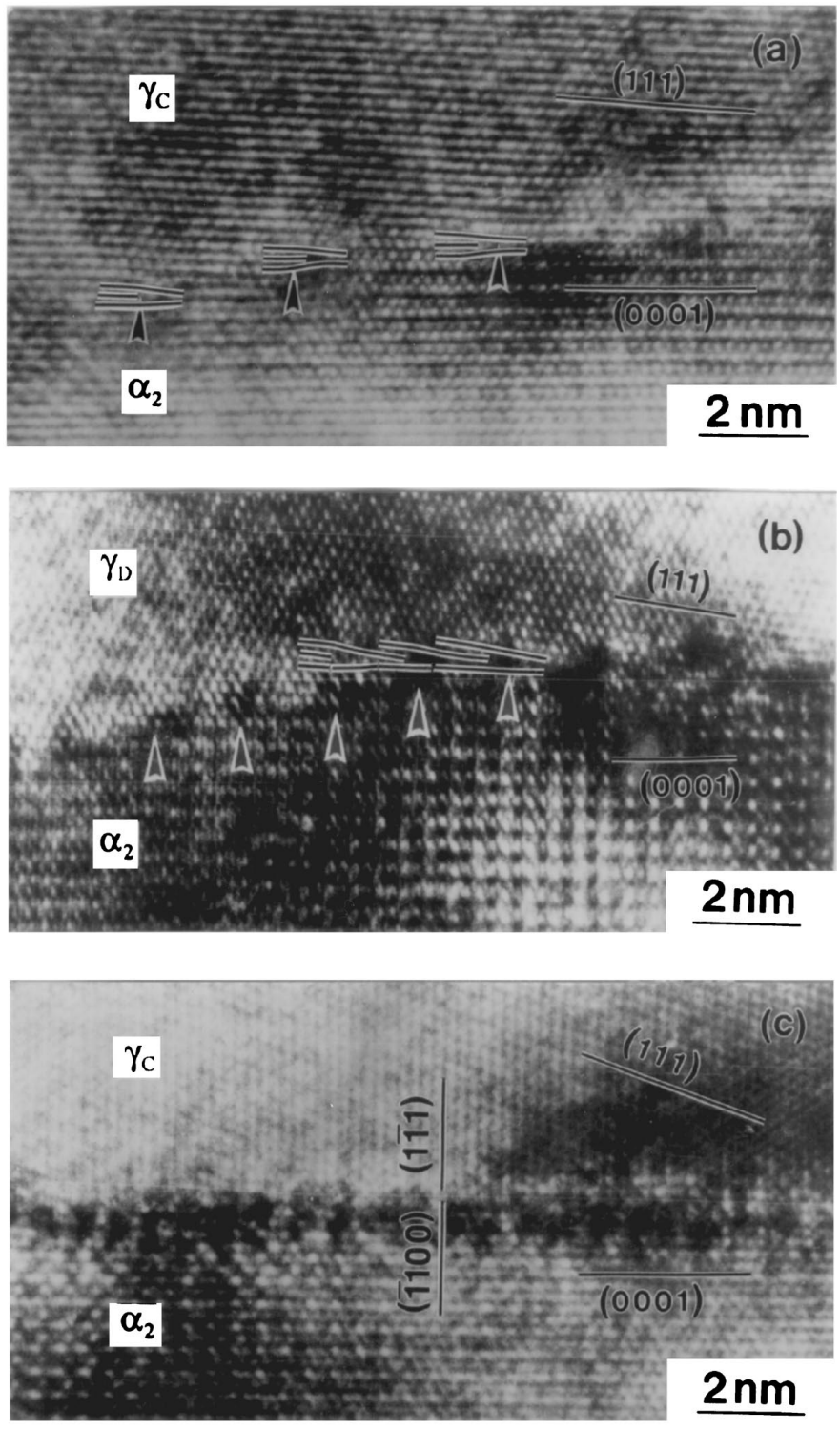

Figure 7 (a)–(c) are the enlargements of Figs 6a–c respectively showing the 1/3[111] partials at the ledges.

are always observed in annealed two-phase TiAl alloys, two types of hot deformation induced special α_2/γ interfaces can also be formed as follows:

(1) coherent interfaces with high density of ledges, the dislocation ledges containing 1/3[111] partials in some ledges.

(2) misoriented semi-coherent α_2/γ interphase boundaries, the density of dislocation ledges in these interfaces increase with the misoriented angle between the $(111)_\gamma$ and $(0001)_{\alpha 2}$ planes, and 1/3[111] partial dislocations were involved in all the dislocation ledges.

3.5. Misoriented semi-coherent α_2/γ interface related deformation process

The deformation was mainly concentrated in the γ lamellae during hot deformation. Extensive twinning and deformation-induced structure transformations were observed in the microstructure during elevated temperature deformation [37, 38]. Misoriented semi-coherent α_2/γ interfaces which are unique characteristic α_2/γ interfaces induced by thermomechanical deformation have been observed to play a very important role on the deformation mechanism in the hot deformation of the present alloy.

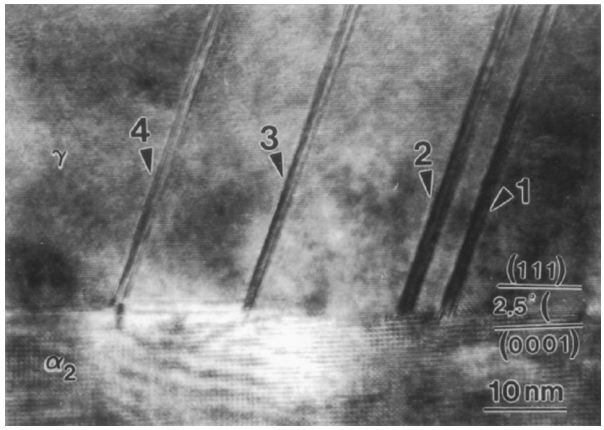

Figure 8 HREM image of deformation twins nucleating at a misoriented semi-coherent α_2/γ interfaces with 2.5° misoriented angle between $(111)_\gamma$ and $(0001)_{\alpha 2}$ planes.

(1) *Deformation twins at the misoriented semi-coherent α_2/γ interface.* Twinning is well accepted as a deformation mode in γ(TiAl) during hot-deformation of two phase alloys. Twins whose twinning plane are $(\bar{1}11)_\gamma$ planes having an angle of about 70.5° with lamellar interfaces usually nucleated at the α_2/γ interface [33]. Fig. 8 demonstrates deformation twins nucleating at a misoriented semi-coherent α_2/γ interface whose misoriented angle between $(111)_\gamma$ and $(0001)_{\alpha 2}$ is about 2.5°, which is similar to the interface in Fig. 6a. The arrows designated with 1, 2, 3 and 4 indicate the twins formed on the α_2/γ interface. These twins are nucleated at the ledges of the misoriented semi-coherent α_2/γ interface, for the ledges can accumulate more stress concentration to favor the nucleation of the twins.

(2) *Deformation induced $\gamma \rightarrow \alpha_2$ structure transformation near the misoriented semi-coherent α_2/γ interface.* The deformation induced structure transformation is a common phenomenon in the deformed two-phase TiAl alloys. Detailed investigations of these deformation induced structure transformations (including $\gamma \rightarrow 9R$, $\gamma \rightarrow \alpha_2$ and $\alpha_2 \rightarrow \gamma$ structure transformations) have been reported elsewhere [34–37]. Here, only the deformation induced $\gamma \rightarrow \alpha_2$ structure transformation near a misoriented semi-coherent α_2/γ interface was demonstrated (in Fig. 9). A deformation induced α_2 phase plate (arrows designated with DI-α_2) which is about 25 nm length and 2.5 nm width is observed in the γ matrix at the upper side of the misoriented semi-coherent α_2/γ interface. The 1/3[111] partial dislocations at the ledges have been observed to move away form the interface to the γ_D matrix. It was suggested that the occurrence of such deformation induced $\gamma \rightarrow \alpha_2$ structure transformation has relation with the moving of the interfacial dislocations during hot working [37].

4. Discussion

4.1. Formation of high density of dislocation ledges in coherent α_2/γ interfaces

In the thermo-equilibrium state, due to the lattice misfit existing in the α_2/γ interface $1/6\langle 11\bar{2}\rangle$ partial dislocations can be introduced in the $(111)_\gamma//(0001)_{\alpha 2}$ interfaces. The formation of the ledge structure at the α_2/γ interface is closely related to these misfit dislocations.

During deformation at elevated temperature, the glide of the high density of mobile interfacial dislocations is a very important deformation mechanism [13, 16, 47]. Usually, the gliding of interfacial dislocations can be retarded by either intrinsic (e.g. existing interfacial ledges and kinks, or solutes and precipitates) or extrinsic (e.g. impinging lattice dislocations) barriers, leading to pile–up configurations. This will increase the interfacial dislocation density and thus increase the ledge density on the α_2/γ interfaces. A high local stress can be generated at these intrinsic or extrinsic barriers as a result of the dislocation pile-up.

On the other hand, moving dislocations in the γ lamellae may inject to the α_2/γ interface and react with interfacial dislocations or dissociate near the α_2/γ interface; it can be considered that the α_2/γ can absorb the slipping dislocations in the γ phase as a dislocation sink. The possible dislocations which can be formed at high-temperature deformation are [110], $[01\bar{1}]$ and $1/2[11\bar{2}]$ types [12–16]. These dislocations can dissociate according to the following ways on (111) planes

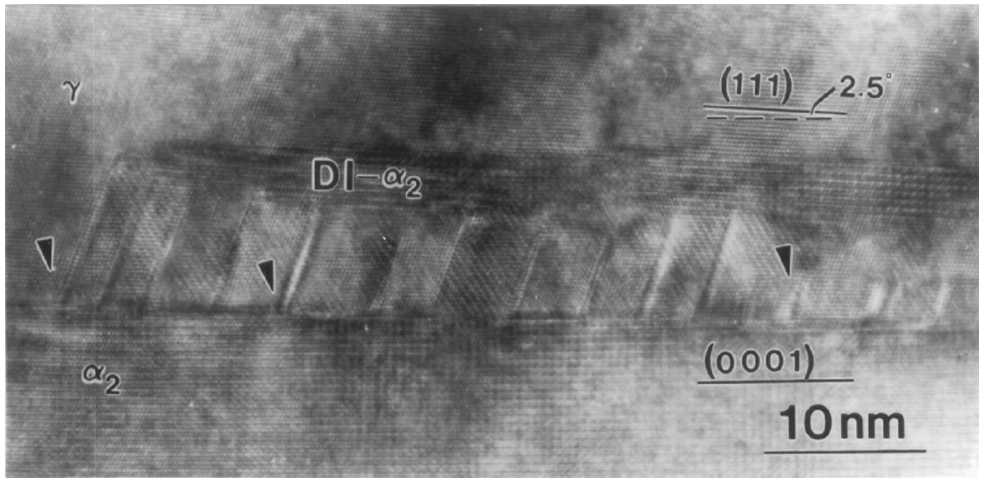

Figure 9 HREM image of the stress-induced $\gamma \rightarrow \alpha_2$ structure transformation near a misoriented semi-coherent α_2/γ interface with 2.5° misoriented angle between $(111)_\gamma$ and $(0001)_{\alpha 2}$ planes.

of TiAl at the α_2/γ interface:

$$1/2[11\bar{2}] \rightarrow 1/6[11\bar{2}] + 1/6[11\bar{2}] + 1/6[11\bar{2}] \quad (1)$$

$$1/2[01\bar{1}] \rightarrow 1/6[\bar{1}2\bar{1}] + 1/6[11\bar{2}] \quad (2)$$

$$1/2[1\bar{1}0] \rightarrow 1/6[1\bar{2}1] + 1/6[2\bar{1}\bar{1}] \quad (3)$$

where, SF represents stacking faults. The coherent α_2/γ interface can act as an effective barrier to the moving dislocations, these dissociated dislocations can be absorbed by the α_2/γ interface. Associated with the existing $1/6\langle 11\bar{2}\rangle$ partial dislocations, these large number of $1/6\langle 11\bar{2}\rangle$ partial dislocations result in the rearrangement of the mismatch interfacial dislocations to accommodate the new interfacial misfit from deformation strain, then the higher density of ledges can be formed in the coherent α_2/γ interface in the high-temperature deformation state.

4.2. Formation of 1/3[111] partial dislocations at α_2/γ interfaces

During the deformation of two-phase ($\gamma + \alpha_2$) alloys, the deformation was mainly concentrated on the γ phases, the moving dislocations can pile-up at the α_2/γ interface. $1/3[111]$ partial dislocation can be introduced by two possible ways at the α_2/γ interface. One is that the moving $1/2[110]$ or $1/2[101](1/2[011])$ dislocations were absorbed at the interface and dissociated at the interface as follows:

$$\begin{aligned} 1/2[110] &\rightarrow 1/3[111] + 1/6[11\bar{2}] \\ 1/2[101] &\rightarrow 1/3[111] + 1/6[1\bar{2}1] \end{aligned} \quad (4)$$

The other is that the moving $1/2[110]$ or $1/2[101]$ $(1/2[011])$ dislocations in the γ phase were hindered near the α_2/γ interface and reacted with $1/6\langle 11\bar{2}\rangle$ partial dislocations at the interface as follows:

$$\begin{aligned} 1/2[110] + 1/6[\bar{1}\bar{1}2] &\rightarrow 1/3[111] \\ 1/2[101] + 1/6[\bar{1}2\bar{1}] &\rightarrow 1/3[111] \end{aligned} \quad (5)$$

By these two ways, the $1/3[111]$ partial dislocations can be introduced at the α_2/γ interface.

Similar $1/3[111]$ partials were also observed at a pseudo-twin boundary between two 120° rotational variants in a Ti-48Al-2Cr alloy by Appel *et al*. [48]. Dislocations of this type are expected to be less efficient in accommodating the rotational misfit and may represent high energy configurations of the interfacial dislocation structure. In single phase γ-TiAl, the total Burgers vector of ordinary dislocation $1/2\langle 110]$, which is expected to dissociate as: $1/2[1\bar{1}0] \rightarrow 1/6[\bar{2}11] +$ CSF $+ 1/6[\bar{1}2\bar{1}]$, is inclined at 60° to the line direction when it was observed along a $[\bar{1}01]$ orientation [49]. In this situation, an extra $(\bar{1}11)$ half-plane can be observed. Because of the extremely high CSF energy, the striking characteristic of this dislocation is the compact nature of the core such that no faulted region is apparent. It is worth noting that in the present observation, the extra half-plane is along the (111) plane not the $(\bar{1}11)$ plane. This suggests that the extra (111) half-plane at the ledges on the α_2/γ interface observed in this study is different from the compact 60° core structure of the $1/2[110]$ ordinary dislocation. The reactions (4) and (5) suggested here are responsible for the formation of these extra (111) half-planes ($1/3[111]$ partial) at the ledges on the α_2/γ interface. Also, because of the extremely high CSF (APB + SISF) energy, the core structure of the total dislocation resulted from the reactions (4) and (5) is highly compact, and no faulted (also APB) region is apparent. The compact nature of the core structure of these dislocations also suggested that a high Peierls stress must exist for their mixed character.

In fact, Pond [50] also observed the dissociation of a lattice dislocation in an incoherent twin boundary of aluminum by reaction (4), and resulting in the formation of 1/3[111] partial dislocation in an incoherent twin boundary. Recently, a similar dislocation configuration was observed in an incoherent twin boundary of aluminum by HREM [51], the Burgers vector was identified as having components $a/3[111] + a/6[\bar{2}11] = a/2[011]$. Also, no APBs or faulted region were observed to be attached with the partial dislocations in these two studies.

As judged from Frank's rule, the reactions (4) and (5) are not energetically feasible. However, the high coherency stresses present at the interfaces may initiate the reactions and support the absorption of the reactant dislocations. During deformation at high temperature, with the help of the thermal activation and the applied stress the reactions (4) and (5) can easily take place.

4.3. Formation of the misoriented semi-coherent α_2/γ interphase boundaries

As discussed in the last part, during the deformation of two-phase ($\gamma + \alpha_2$) alloys, the $1/3[111]$ partial dislocation can be introduced either by the dissociation of $1/2\langle 110\rangle$ dislocations at the interface or by the reaction of $1/2\langle 110\rangle$ with $1/6\langle 11\bar{2}\rangle$ at the interface. The characteristics of whole ledge dislocations containing $1/3[111]$ partial can be characterized as $1/6\langle 112\rangle$ partial dislocation $+1/3[111]$ partial dislocation.

A glide or climb dislocation associated with a ledge introduces a displacement parallel or normal respectively, to the interface [52]. Therefore a ledge can move in an interface by diffusion of atoms across the ledge together with glide or climb of any associated dislocations. A displacement non-parallel to the interface plane requires a climb dislocation at the ledge and subsequently the interface is displaced perpendicular to itself. A ledge which contains a glide dislocation alters only the average orientation of the interface as it moves whereas a ledge with a climb dislocation alters the lattice orientation across the interface and the average interface orientation. In the present case in Figs 6 and 7, $1/3[111]$ partial dislocations are of climb character, the observed deviation of the lattice orientation across the interface obviously comes from these ledges with climb dislocations ($1/3[111]$ partial dislocations). The similar deviation of the lattice orientation across the interface, which resulted from a regular array of

edge dislocation $1/3[111]_{fcc}$ at the interface, was observed by Penisson and Regheere [53] at a f.c.c./b.c.c. interface in an iron-based stainless steel.

In fact, the deviation of the overall habit plane from $(111)_\gamma//(0001)_{\alpha 2}$ can also be observed (see Fig. 6). This is because the Burgers vector of the dislocation associated with the ledge is $1/2[110]$, and the configuration of the ledge dislocation is the dissociation of this $1/2[110]$, i.e. $1/2[110] \rightarrow 1/3[111] + 1/6[11\bar{2}]$, the ledges at the interface contain both climb ($1/3[111]$) and glide ($1/6[11\bar{2}]$) dislocations, therefore the overall habit plane from $(111)_\gamma//(0001)_{\alpha 2}$ can be deviated accompanied with the deviation of the lattice orientation across the interface. That means the interface is not a pure tilt interface. However, considering the deviation of the overall habit plane from $(111)_\gamma//(0001)\alpha 2$ is much smaller compared with the deviation of the lattice orientation across the interface, the interfaces in Fig. 6 can be approximately treated as a pure tilt interface. The mean separation between dislocations in the boundary can be calculated according to the $1/3[111]$ equation: $D = b/2\sin(\theta/2)$ [54]. With $b(1/3[111]) = 0.231$ nm and $\theta = 2.51^\circ$, 8.0°, and 18.5°, the calculated D values equal to 5.29, 1.66, and 0.72 nm respectively, which are consistent with the measured values.

4.4. Possible roles of α_2/γ interfaces on the deformation of two-phase TiAl alloys

As elucidated in the last three parts, during the deformation at high temperature, the interfacial dislocations (the ledges) are rearranged by the gliding of the mobile interfacial dislocations and the reaction of lattice dislocations with the interfacial dislocations to accommodate the new interfacial misfit from the deformation strain. Then both coherent interfaces with high density of ledges and misoriented semi-coherent α_2/γ interfaces can be produced. This process can be regarded as that the α_2/γ interface can absorb the moving dislocations in the γ phase as a dislocation sink. On the other hand, the as-received complex interfacial dislocation structures during high temperature deformation can also play an important role in the deformation process in the γ phase lamellae. For example, ordinary dislocation loops with Burgers vector $\mathbf{b} = 1/2\langle 110]$ were observed to emit from the semi-coherent twin-related γ/γ boundaries, and microtwins were observed to nucleate heterogeneously at misfit interfacial dislocations [17, 48]. In the present study, formation of deformation twins and deformation-induced structure transformation can be observed as an interface-related process (see Figs 8 and 9). Several mechanisms, such as, ledge dislocation dissociation mechanism [30], stair-rod cross-slip reaction mechanism [47] and $1/3[111]$ partial dissociation ($1/3[111] \rightarrow 1/6[112] + 1/6[110]$) mechanism [48] have been proposed to explain the formation of deformation twins at interface. The occurrence of the $\gamma \rightarrow \alpha_2$ structure transformation can also be explained as a result of the movement of the $1/3[111]$ interfacial dislocations away from the interface to the interior of the γ phase lamellae during high temperature deformation [37]. All these interface-related deformation process can be regarded as that the α_2/γ interface can also emit dislocations as a dislocation source during high temperature deformation. Thus, the structural characteristics of the α_2/γ lamellar interfaces have very important effects on the deformation behavior of two-phase TiAl alloys. Therefore, the modification of the structural characteristics of the α_2/γ lamellar interfaces by thermomechanically processing may result in the improvement of the mechanical properties of the two-phase TiAl alloys.

5. Conclusions

The structure modifications on α_2/γ interface induced by deformation in a hot-deformed Ti-45Al-10Nb alloy were investigated by conventional and high-resolution transmission electron microscopy.

A new type of dislocation ledge containing $1/3[111]$ partials was identified. The Burgers vectors of these dislocation ledges were determined to be $1/2[110]$ or $1/2\langle 101]$. $1/3[111]$ partials can be introduced to the ledges either by the dissociation of $1/2[110]$ dislocations at the interface or by the reaction of $1/2[110]$ with $1/6[\bar{1}12]$ at the interface.

Two types of hot deformation induced α_2/γ interfaces can be formed as follows:

(1) coherent interfaces with high density of ledges, the dislocation ledges containing $1/3[111]$ partials in some ledges.

(2) misoriented semi-coherent α_2/γ interphase boundaries, the density of dislocation ledges in these interfaces increase with the misoriented angle between the $(111)_\gamma$ and $(0001)_{\alpha 2}$ planes, and $1/3[111]$ partial dislocations were involved in all the dislocation ledges.

The formation mechanism of these deformation-induced α_2/γ interfaces were suggested as a result of the gliding of the mobile interfacial dislocations and the reaction of lattice dislocations with the interfacial dislocations to accommodate the new interfacial misfit from the deformation strain. This relates to the role of α_2/γ interfaces adjusting the deformation as a dislocation sink absorbing the moving dislocations in the γ phase. Moreover, misoriented semi-coherent α_2/γ interface related deformation twinning and deformation-induced structure transformation were analyzed and discussed related to the role of α_2/γ interfaces as a dislocation source during deformation.

The deformation behavior of two-phase TiAl alloys are strongly dependent on the α_2/γ lamellar interfaces. Therefore, the modification of the structural characteristics of the α_2/γ lamellar interfaces by thermomechanically processing may be a possible way for the improvement of the mechanical properties of the two-phase TiAl alloys.

Acknowledgements

This work was partly supported by the National Nature Sciences Foundation of China (NNSFC) and a research grant from the Laboratory of Atomic Imaging of Solids, Institute of Metal Research, Academia Sinica.

References

1. E. L. HALL and S. C. HUANG, *J. Mater. Res.* **4** (1989) 595.
2. *Idem.*, in "High Temperature Ordered Intermetallic Alloys III," Materials Research Society Symposium Proceedings, Vol. 133, edited by C. T. Liu, A. I. Taub, N. S. Stoloff and C. C. Koch (Materials Research Society, Pittsburgh, Pennsylvania, 1989), p. 693.
3. N. K. VASUDEVAN, M. A. STUCKE, S. A. COURT and H. L. FRASER, *Phil. Mag. Lett.* **59** (1989) 299.
4. Y. W. KIM, *JOM* **41**(7) (1989) 24.
5. Y. W. KIM and D. M. DIMIDUK, *ibid.* **43**(8) (1991) 40.
6. Y. W. KIM, *ibid.* **46**(7) (1994) 30.
7. M. YAMAGUCHI and H. INUI, in "Structural Intermetallics," edited by R. Darolia, J. J. Lewandawski, C. T. Liu, P. L. Martin, D. B. Miracle and M. V. Nathal (The Minerals, Metals & Materials Society, 1993) p. 127.
8. M. J. BLACKBURN, in "Technology and Application of Titanium," edited by R. T. Jaffee and N. E. Promisel (Pergamon Oxford, 1970), p. 633.
9. T. KAWABATA, M. TANADO and O. IZUMI, *Scripta Metall.* **22** (1988) 1725.
10. S. C. HUANG and E. L. HALL, *Metall. Trans. A* **22** (1991) 427.
11. C. R. FENG, D. J. MICHEL and C. R. CROWE, *Scripta Metall.* **23** (1989) 1707.
12. W. WUNDERLICH, G. FROMMEYER and P. V. CZARNOWSKI, *Mater. Sci. Eng. A* **164** (1993) 421.
13. W. WUNDERLICH, TH. KREMSER and G. FROMMEYER, *Acta Metall. Mater.* **41** (1993) 1791.
14. L. ZHAO and K. TANGRI, *Phil. Mag. A* **64** (1991) 361.
15. *Idem.*, *Acta Metall.* **39** (1991) 2209.
16. *Idem.*, *Phil. Mag. A* **65** (1992) 1065.
17. F. APPEL, P. A. BEAVEN and R. WAGNER, *Acta Metall. Mater.* **41** (1993) 1721.
18. L. L. HE, H. Q. YE, X. G. NING, M. Z. CAO and D. HAN, *Phil. Mag. A* **67** (1993) 1161.
19. H. INUI, A. NAKAMURA, M. H. OH and M. YAMAGUCHI, *Ultramicroscopy* **39** (1991) 268.
20. H. INUI, M. H. OH, A. NAKAMURA and M. YAMAGUCHI, *Phil. Mag. A* **66** (1992) 539.
21. G. J. MAHON and J. M. HOWE, *Metall. Trans. A* **21** (1990) 1655.
22. J. M. PENISSON, *Mater. Sci. Forum* **126–128** (1993) 35.
23. J. M. PENISSON, R. BONNET, M. LOUBRADOU and C. DERDER, *Mater. Res. Soc. Symp. Proc.* **238** (1992) 41.
24. J. M. PENISSON, M. LOUBRADOU, C. DERDER and R. BONNET, *Mater. Sci. Forum* **126–128** (1993) 141.
25. O. POPOOLA, C. CORDIER, P. PIROUZ and A. H. HEUER, *Scripta Metall. Mater.* **26** (1992) 1643.
26. S. R. SINGH and J. M. HOWE, *Scripta Metall. Mater.* **25** (1991) 485.
27. S. R. SINGH and J. M. HOWE, in "High Temperature Ordered Intermetallic Alloys IV," Materials Research Society Symposium Proceedings (Materials Research Society, Pittsburgh, Pennsylvania, 1991) Vol. 213, p. 435.
28. S. R. SINGH and J. M. HOWE, *Phil. Mag. Lett.* **65** (1992) 233.
29. *Idem.*, *Phil. Mag. A* **66** (1992) 739.
30. Y. S. YANG and S. K. WU, *ibid.* **67** (1993) 463.
31. G. L. CHEN, W. J. ZHANG, Y. D. WANG, J. G. WANG and Z. Q. SUN, in "Structural Intermetallics," edited by R. Darolia, J. J. Lewandawski, C. T. Liu, P. L. Martin, D. B. Miracle and M. V. Nathal (The Minerals, Metals & Materials Society, 1993) p. 319.
32. G. L. CHEN, J. G. WANG, L. C. ZHANG and H. Q. YE, *Acta Metall. Sinica* **8** (1995) 273.
33. J. G. WANG, L. C. ZHANG, G. L. CHEN and H. Q. YE, in "Structural Intermetallics 1997," edited by M. V. Nathal, R. Darolia, C. T. Liu, P. L. Martin, D. B. Miracle, R. Wagner and M. Yamaguchi (The Minerals, Metals and Materials Society, Warrendale, PA, 1997) p. 119.
34. J. G. WANG, G. L. CHEN, L. C. ZHANG and H. Q. YE, *Materials Letters* **31** (1997) 179.
35. *Idem.*, *Scripta Metall. Mater.* **37** (1997) 135.
36. *Idem.*, *Mater. Sci. Eng. A* **A239–240** (1997) 287.
37. *Idem.*, *J. Mater. Sci.* **33** (1998) 2563.
38. *Idem.*, *Mater. Sci. Eng. A* **A252** (1998) 222.
39. *Idem.*, *Intermetallics* **5** (1997) 289.
40. J. G. WANG, PhD thesis, University of Science and Technology, Beijing, 1994.
41. D. G. KONITZER, I. P. JONES and H. L. FRASER, *Scripta Metall.* **20** (1986) 265.
42. C. R. FENG, D. J. MICHEL and C. R. CROWE, *ibid.* **22** (1988) 1481.
43. *Idem.*, *Phil. Mag. Lett.* **61** (1990) 95.
44. Y. S. YANG and S. K. WU, *Scripta Metall. Mater.* **24** (1990) 1801.
45. *Idem.*, *Phil. Mag. A* **65** (1992) 15.
46. J. M. HOWE, U. DAHMEN and R. GRONSKY, *ibid.* **56** (1987) 31.
47. L. M. HSIUNG and T. G. NIEH, in "Structural Intermetallics 1997," edited by M. V. Nathal, R. Darolia, C. T. Liu, P. L. Martin, D. B. Miracle, R. Wagner and M. Yamaguchi (The Minerals, Metals and Materials Society, Warrendale, PA, 1997) p. 129.
48. F. APPEL and R. WAGNER, in "Atomic Resolution Microscopy of Surfaces and Interfaces," edited by D. J. Smith, Materials Research Society Symposium Proceedings (Materials Research Society, Pittsburgh, Pennsylvania, 1997) Vol. 466, p. 145.
49. M. J. MILLS, J. M. K. WIEZOREK and H. L. FRASER, in "Atomic Resolution Microscopy of Surfaces and Interfaces," edited by D. J. Smith, Materials Research Society Symposium Proceedings (Materials Research Society, Pittsburgh, Pennsylvania, 1997) Vol. 466, p. 131.
50. R. C. POND, *Proc. Roy. Soc. Lond. A* **357** (1977) 453.
51. D. L. MEDLIN, C. B. CARTER, J. E. ANGELO and M. J. MILLS, *Phil. Mag. A* **75** (1997) 733.
52. J. P. HIRTH and R. W. BALLUFFI, *Acta Metall.* **21** (1973) 929.
53. J. M. PENISSON and G. REGHEERE, *Mater. Sci. Eng. A* **107** (1989) 199.
54. J. P. HIRTH and J. LOTHE, "Theory of Dislocation," 2nd ed. (Wiley, New York, 1982) p. 705.

Received 17 April 1998
and accepted 24 May 1999